Year: 2018

Germinal centers determine the prognostic relevance of tertiary lymphoid structures and are impaired by corticosteroids in lung squamous cell carcinoma

Silina, Karina ; Soltermann, Alex ; Movahedian Attar, Farkhondeh ; Casanova, Ruben ; Uckeley, Zina M ; Thut, Helen ; Wandres, Muriel ; Isajevs, Sergejs ; Cheng, Phil ; Curioni Fontecedro, Alessandra ; Foukas, Periklis ; Levesque, Mitchell P ; Moch, Holger ; Linē, Aija ; van den Broek, Maries

Abstract: In solid tumors, the presence of lymph node-like structures called tertiary lymphoid structures (TLS) is associated with improved patient survival. However, little is known about how TLS form in cancer, how their function affects survival, and whether they are affected by cancer therapy. In this study, we used multi-spectral microscopy, quantitative pathology and gene expression profiling to analyze TLS formation in human lung squamous cell carcinoma (LSCC) and in an experimental model of lung TLS induction. We identified a niche of CXCL13+ perivascular and CXCL12+LTB+ and PD-L1+ epithelial cells supporting TLS formation. We also characterized sequential stages of TLS maturation in LSCC culminating in the formation of germinal centers (GC). In untreated patients, TLS density was the strongest independent prognostic marker. Further, TLS density correlated with GC formation and expression of adaptive immune response-related genes. In patients treated with neoadjuvant chemotherapy, TLS density was similar but GC formation was impaired and the prognostic value of TLS density was lost. Corticosteroids are co-administered with chemotherapy to manage side effects in LSCC patients, so we evaluated whether they impaired TLS development independently of chemotherapy. TLS density and GC formation were each reduced in chemotherapy-naive LSCC patients treated with corticosteroids before surgery, compared to untreated patients, a finding that we confirmed in the experimental model of lung TLS induction. Overall, our results highlight the importance of GC formation in TLS during tumor development and treatment.

DOI: https://doi.org/10.1158/0008-5472.CAN-17-1987

Originally published at:
Silina, Karina; Soltermann, Alex; Movahedian Attar, Farkhondeh; Casanova, Ruben; Uckeley, Zina M; Thut, Helen; Wandres, Muriel; Isajevs, Sergejs; Cheng, Phil; Curioni Fontecedro, Alessandra; Foukas, Periklis; Levesque, Mitchell P; Moch, Holger; Linē, Aija; van den Broek, Maries (2018). Germinal centers determine the prognostic relevance of tertiary lymphoid structures and are impaired by corticosteroids in lung squamous cell carcinoma. Cancer Research, 78(5):1308-1320.
DOI: https://doi.org/10.1158/0008-5472.CAN-17-1987

Germinal centers determine the prognostic relevance of tertiary lymphoid structures and are impaired by corticosteroids in lung squamous cell carcinoma

Karīna Siliņa[1], Alex Soltermann[2], Farkhondeh Movahedian Attar[1], Ruben Casanova[2], Zina M. Uckeley[1], Helen Thut[1], Muriel Wandres[1], Sergejs Isajevs[3,4], Phil Cheng[5], Alessandra Curioni-Fontecedro[6], Periklis Foukas[7,8], Mitchell P. Levesque[5], Holger Moch[2], Aija Linē[9], Maries van den Broek[1*]

[1]Institute of Experimental Immunology, University of Zurich, Switzerland

[2]Institute of Pathology and Molecular Pathology, University Hospital Zurich, Switzerland

[3]Pathology Center, Riga East Clinical University Hospital, Riga, Latvia

[4]Faculty of Medicine, University of Latvia, Latvia

[5]Department of Dermatology, University Hospital Zurich, Switzerland

[6]Department of Oncology, University Hospital Zurich, Switzerland

[7]Department of Oncology, CHUV-UNIL, Switzerland

[8]Department of Pathology, Attikon University Hospital, National and Kapodistrian University of Athens, Greece

[9]Latvian Biomedical Research and Study Center, Latvia

Running title: Steroids impair tertiary lymphoid structures in lung cancer

Correspondence to: Prof. Maries van den Broek vandenbroek@immunology.uzh.ch, Institute of Experimental Immunology, University of Zurich, Zurich, CH-8057, Switzerland, Phone +41 44 635 3722

Conflict of interest statement: The authors declare no potential conflicts of interest.

Author Manuscript Published OnlineFirst on December 26, 2017; DOI: 10.1158/0008-5472.CAN-17-1987
Author manuscripts have been peer reviewed and accepted for publication but have not yet been edited.

List of Abbreviations

TLS – tertiary lymphoid structure

E-TLS – early TLS

PFL-TLS – primary follicle-like TLS

SFL-TLS – secondary follicle-like TLS

GC – germinal center

LSCC – lung squamous cell carcinoma

NSCLC – non-small cell lung cancer

HEV – high endothelial venule

DC – dendritic cell

FDC – follicular dendritic cell

LT – lymphotoxin

T_{FH} – T follicular helper cell

Treg – T regulatory cell

TIL – tumor infiltrating lymphocyte

SLO – secondary lymphoid organ

iBALT – inducible bronchus associated lymphoid tissue

COPD – chronic obstructive pulmonary disease

FFPE – formalin-fixed paraffin-embedded

HPF – high-power field

H&E – hematoxylin and eosin

IHC – immunohistochemistry

IF – immunofluorescence

ROC – Receiver Operating Characteristics

PFS – progression-free survival

DFS – disease-free survival

DSS – disease-specific survival

OS – overall survival

HR – hazard ratio

Author Manuscript Published OnlineFirst on December 26, 2017; DOI: 10.1158/0008-5472.CAN-17-1987
Author manuscripts have been peer reviewed and accepted for publication but have not yet been edited.

ABSTRACT

In solid tumors, the presence of lymph node-like structures called tertiary lymphoid structures (TLS) is associated with improved patient survival. However, little is known about how TLS form in cancer, how their function affects survival, and whether they are affected by cancer therapy. In this study, we used multi-spectral microscopy, quantitative pathology and gene expression profiling to analyze TLS formation in human lung squamous cell carcinoma (LSCC) and in an experimental model of lung TLS induction. We identified a niche of CXCL13+ perivascular and CXCL12+LTB+ and PD-L1+ epithelial cells supporting TLS formation. We also characterized sequential stages of TLS maturation in LSCC culminating in the formation of germinal centers (GC). In untreated patients, TLS density was the strongest independent prognostic marker. Further, TLS density correlated with GC formation and expression of adaptive immune response-related genes. In patients treated with neoadjuvant chemotherapy, TLS density was similar but GC formation was impaired and the prognostic value of TLS density was lost. Corticosteroids are co-administered with chemotherapy to manage side effects in LSCC patients, so we evaluated whether they impaired TLS development independently of chemotherapy. TLS density and GC formation were each reduced in chemotherapy-naive LSCC patients treated with corticosteroids before surgery, compared to untreated patients, a finding that we confirmed in the experimental model of lung TLS induction. Overall, our results highlight the importance of GC formation in TLS during tumor development and treatment.

PRECIS

Corticosteroid treatment during chemotherapy negatively affects the development of tertiary lymphoid structures and abrogates their prognostic value in lung cancer patients.

Author Manuscript Published OnlineFirst on December 26, 2017; DOI: 10.1158/0008-5472.CAN-17-1987
Author manuscripts have been peer reviewed and accepted for publication but have not yet been edited.

INTRODUCTION

Tertiary lymphoid structures (TLS) resemble follicles of secondary lymphoid organs (SLO) both by structure and function and develop in response to chronic inflammation (1) and cancer (2,3). The presence of germinal centers (GC) within TLS correlates with exacerbated autoimmunity and transplant rejection due to the generation of auto-reactive B cells and high endothelial venules (HEVs) (1). In models for infection TLS serve as priming sites for T cells and contribute to pathogen clearance (4,5). The first prognostic analysis of TLS in human cancer showed that TLS containing GC correlate with improved survival for patients with hepatocellular carcinoma (6). Further studies showed that either total TLS numbers or the numbers of TLS-associated immune cells including follicular helper T (T_{FH}) cells, follicular B cells, mature dendritic cells (DCs) and HEVs are associated with prolonged survival in many different tumor types (3,7-10). Specifically in non-small cell lung cancer (NSCLC), the number of CD208+ (DC-LAMP+) antigen presenting mature DCs, which reside in T cell areas of TLS, significantly correlated with improved survival (11), especially in combination with the number of CD8+ T cells (12) or follicular B cells (13). Tumor-associated TLS provide the necessary specialized vasculature and chemo-attractants that allows T cell infiltration (14) and significantly correlate with tumor-infiltrating T cells and plasma cells (13,15,16). B cell and T cell receptor sequencing data show clonal expansion of lymphocytes in tumor-associated TLS suggesting a direct role for TLS in the priming of anti-tumor immunity (17-19). Moreover, the application of CXCL13 or lymphotoxin (LT) – two components of a positive feedback-loop orchestrating the organogenesis of SLO (20) and TLS development in adult mice (21) – resulted in tumor control in models of colorectal cancer (CRC) (22) or melanoma (23). In order to normalize tumor-associated blood vessels, Johansson-Percival *et al.* delivered LIGHT to such vessels resulting in susceptibility of RIP-

Author Manuscript Published OnlineFirst on December 26, 2017; DOI: 10.1158/0008-5472.CAN-17-1987
Author manuscripts have been peer reviewed and accepted for publication but have not yet been edited.

TAg pancreatic tumors to treatment with anti-cancer vaccines and immune checkpoint inhibition. Interestingly, targeting LIGHT to tumor-associated blood vessels induced formation of TLS, which can be explained by the fact that LIGHT is an essential ligand for SLO and TLS development (24). In human pancreatic ductal adenocarcinoma, TLS developed in response to GVAX immunotherapy in around 85% of patients and their presence is associated with an increased ratio of intratumoral Teffector:Treg cells, improved post-vaccination responses and prolonged survival (25).

In light of these studies, deliberate induction of tumor-associated TLS has been proposed as a novel immunotherapeutic approach (2,3). However, the mechanisms underlying TLS development in different human tissues are poorly understood and may be affected by the nature of the inflammatory stimulus and the organ-specific environments (7). In lungs for example, viral or bacterial stimuli activate the LT/CXCL13 or IL-17/CXCL12 pathway, respectively, resulting in the formation of TLS, also known as inducible bronchus associated lymphoid tissue (iBALT) (26). The LT/CXCL13 pathway is crucial for differentiation of follicular dendritic cells (FDC) and functional GC (26,27). Both pathways participate in TLS development in response to cigarette smoke or LPS, which is a major component of cigarette smoke (28), in patients and animal models of chronic obstructive pulmonary disease (COPD) (29,30). Cigarette smoke and inhaled particulates such as alum drive the release of IL1α by alveolar macrophages and lead to iBALT formation (31-33). Additional factors like CCL19, CCL21 and IL-22 also contribute to iBALT development (34,35) but which stimuli are upstream of these pathways is not known. A crucial role for B cells, T cells and DC in the generation and maintenance of TLS has been demonstrated in various animal models (35). Finally, Krautler et al. showed that ubiquitous perivascular PDGFRβ^{+} mesenchymal cells are the precursors of FDCs, which orchestrate B cell accumulation and TLS development in a LTβ receptor (LTBR)-dependent manner explaining why TLS can arise in any vascularized organ (36). The abovementioned chemokines and immune cells are linked to the presence of

Author Manuscript Published OnlineFirst on December 26, 2017; DOI: 10.1158/0008-5472.CAN-17-1987
Author manuscripts have been peer reviewed and accepted for publication but have not yet been edited.

TLS in human cancers (3,37). However, there is little information about the sequence of events that drive the development of tumor-associated TLS or about which features of TLS are relevant for patients' survival. To address these questions we characterized the TLS-associated microenvironment and TLS composition in human LSCC tissues and an experimental model of lung TLS induction. We identified three distinct maturation stages of TLS culminating in GC formation with significant relevance for patient survival and expression of adaptive immunity-related genes. Corticosteroids are frequently used to manage side effects of chemo- or radiotherapy or to treat other co-morbidities of cancer patients. Our data suggest that corticosteroids have a negative impact on TLS development and specifically on GC formation in LSCC patients and lungs of mice.

METHODS

Patient material

Patient analyses were conducted according to the Declaration of Helsinki. Ethical approval for performing research on anonymized, archival patient material was obtained from the cantonal ethics commission Zurich (KEK-ZH-2013-0584 amendment 26.11.2015, KEK-ZH-29-2009 amendment 20.05.2016) and Ethics Committee of Biomedical Research of Riga East University Hospital with signed informed consents.

Samples from patients who underwent resection of LSCC regardless of tumor stage in University Hospital Zurich (USZ) were collected between 2003 and 2010, and were analyzed for their baseline and outcome clinical information retrospectively from the in-house diagnostic and treatment databases (n=245) by a clinical pathologist (AS) and a medical oncologist (ACF). Following criteria were used to exclude patients: Mixed tumor histology, prior diagnosis of a squamous cell carcinoma of head and neck or incomplete diagnostic and clinical data. Patients who passed the exclusion criteria were sorted by tumor stage and similar proportions of early and late stage patients were selected for analysis (Zurich cohort, n=138, **Table 1**). These patients were followed-up until December 2015 (median follow-up time from diagnosis 1429 days).

Information on patients who underwent resection of lung cancer in Riga Eastern Clinical University Hospital (Riga cohort, n=78) is provided in Supplementary methods and **Supplementary Table S1**.

Histological evaluation

The number of dense lymphocytic aggregates was quantified per 10x high-power field (HPF) in all tumor-containing hematoxylin and eosin (H&E)-stained diagnostic sections of the Zurich cohort. TLS density was calculated as the number of TLS per mm^2 in peritumoral and intratumoral regions. A patient was considered as GC-positive if at least one TLS showed the characteristic morphology of proliferating centroblasts. The sample analyst (KS) was blinded for the patients' clinical data at the time of histological evaluation. Further details provided in Supplementary methods.

Gene expression analysis

A representative set of 27 chemotherapy-naïve patients was selected to match the whole cohort for the variability of TLS density, survival and stage and included 10 TLS-low and 17 TLS-high tumors. Full details on tissue preparation and qPCR data analysis according to the MIQE guidelines (38) are provided in Supplementary methods and **Supplementary Fig. S1A** and **B**. Primer sequences are shown in **Supplementary Table S2**.

Immunostaining and quantitative pathology

Antibodies and detection reagents used for immunostaining are listed in **Supplementary Table S3**. Full details on immunohistochemical (IHC) and immunofluorescent (IF) staining protocols are provided in Supplementary methods. To analyze TLS maturation in different TLS density groups a set of 61 chemotherapy-naïve patients was selected to match the whole cohort for the variability of TLS density, survival and stage and included 24 TLS-low and 37 TLS-high tumors (**Supplementary Fig. S1C**). To analyze the effects of neoadjuvant treatments 28 TLS-high patients treated with neoadjuvant chemotherapy (Zurich cohort) and all TLS-high patients that received neoadjuvant radiotherapy (Riga cohort, n=4) were selected. To analyze the effects of corticosteroids, chemotherapy-naïve patients of the Zurich cohort that had received corticosteroids before surgery to treat other comorbidities (n=15, **Supplementary Table S4**) were compared to patients without any steroid or chemotherapy treatment (n=43).

For TLS maturation analysis slides were co-stained for CD21, CD23, and CXCL13. All dense lymphocytic aggregates irrespective of CD21/CD23 signal were imaged as multispectral HPF (200x) by Vectra 3.0 imaging system (PerkinElmer). Spectral unmixing is described in Supplementary methods. Each HPF image was evaluated for the TLS maturation stage as follows: early TLS (E-TLS), dense lymphocytic aggregates lacking CD21 and CD23 signal; primary follicle-like TLS (PFL-TLS), dense lymphocytic aggregates with CD21 but no CD23 signal; secondary follicle-like TLS (SFL-TLS), dense lymphocytic aggregates with CD21 and CD23 signal. The proportion of TLS in each maturation stage was determined for each patient. To determine the size of GC, tissue segmentation algorithm of Inform software (PerkinElmer) was trained to recognize areas that co-expressed CD21 and CD23. The GC size was calculated as the average pixel count per GC area for each patient. Segmentation quality was verified for all images by the sample analyst (KS) who was blinded for the patients' clinical data at the time of image analysis. Inappropriately segmented images were excluded from calculations. For the analysis of DCs and HEVs in the context of TLS maturation slides were co-stained for CD20, CD21, CD23, PNAD and DC-LAMP. All dense lymphocytic aggregates and all areas with PNAD and DC-LAMP signal were imaged and analyzed as above.

Author Manuscript Published OnlineFirst on December 26, 2017; DOI: 10.1158/0008-5472.CAN-17-1987
Author manuscripts have been peer reviewed and accepted for publication but have not yet been edited.

In vivo experiments

All animal experiments were approved by the cantonal veterinary office Zurich (license number 127/2015) and conducted in accordance to the Swiss federal and cantonal law on animal protection. Female C57BL/6NRj mice (8-12-weeks-old) were obtained from Janvier Labs (Saint Berthevin, France) and maintained in specific pathogen-free facilities at the University of Zurich. Mice received intranalsal (i.n.) administration of alum ovalbumin (Ova) as described before (33) and received daily p.o. dexamethasone (0.3 mg/kg) or PBS. Full details on treatment protocols and analysis are provided in Supplementary methods.

Statistics

Statistical analyses were performed using RStudio (V1.0.44) software. The threshold of TLS density was identified using the Receiver Operating Characteristics (ROC) curve analysis. Three years of PFS was set as the discriminant for short- and long-term survival. Neoadjuvant chemotherapy-treated patients (n=51) as well as chemotherapy-naïve patients whose follow-up was shorter that 3 years without relapse (n=8) where excluded from this analysis. The prognostic significance of TLS density was assessed by the Kaplan-Meier curve, univariate and multivariate Cox regression analyses. Patients who died up to one month after surgery (n=6) were excluded from progression-free (PFS) and disease-free survival (DFS) analysis. PFS was calculated from date of surgery for patients with complete resection (R0) (n=121) or from the end date of adjuvant therapy for R>0 patients (n=11) until diagnosis of relapse. DFS was analyzed for R0 patients without pleural infiltration (n=118) from the date of surgery until the date of relapse. Disease-specific (DSS) and overall survival (OS) was defined as the number of days from surgery until death and was analyzed for all patients (n=138). Diagnosis of relapse or cancer-related death were considered as events for the PFS/DFS and DSS/OS analysis, respectively. Patients were censored at the day of last follow-up if lost from follow-up, diagnosed with a new unrelated tumor, died of a cancer non-related cause (not for OS), were alive (for DSS/OS) and not relapsed (for DFS/PFS).

Quantification data are presented in dot plots with interquartile ranges and Turkey whiskers, or percent bar plots. Two-tailed Wilcoxon rank-sum test was used to compare all measured parameters between LSCC patient groups. For gene expression analysis, the Benjamini-and-Hochberg method was used to correct the *p* values for multiple testing. The correlation between gene expression, histological and clinical parameters was assessed by the Spearman's correlation or $\chi 2$ test with Yates' correction.

Multiple group comparison was done as follows: Quantification of TLS maturation in chemotherapy-naïve patients vs. neoadjuvant chemotherapy and radiotherapy-treated patients was compared by Kruskal-Wallis test with Dunn's multiple comparison test. For the mouse experiment, groups were compared by the one-way ANOVA with Dunnett's multiple comparison test. Alum only mice (group 2) were compared to negative control mice (group 1) and alum + Ova mice (group 3). Alum + Ova mice (group 3) were compared to alum only (group 2) and dexamethasone-treated mice (group 4).

RESULTS

The development of tumor-associated TLS follows sequential stages of maturation

We initially assessed the presence of TLS in H&E-stained primary LSCC tissues using full diagnostic cases of 138 patients from the University Hospital Zurich (**Table 1**). We defined TLS as dense lymphocytic clusters and found that >95% of tumors contain such structures predominantly in the tumor periphery (**Fig. 1A-C**), especially in the broncho-alveolar tissues (**Fig. 1D**). In about 50% of tumors, we found TLS with a characteristic morphology of GC (**Fig. 1A**, arrowheads). Because such GC-containing TLS were highly similar to the secondary follicles in SLO (**Fig. 1E, F**) we proposed that TLS without GC represent the

Author Manuscript Published OnlineFirst on December 26, 2017; DOI: 10.1158/0008-5472.CAN-17-1987
Author manuscripts have been peer reviewed and accepted for publication but have not yet been edited.

analogues of the lymph node primary follicles, which contain mature FDC networks but lack GC. We used multi-parameter immunofluorescence (IF) to test this in serial LSCC sections spanning a depth of 250 μm. Indeed, TLS containing mature CD21$^+$ FDC and lacking GC (CD23$^-$) were present in the lungs of LSCC patients (**Fig. 1G**). Moreover, we observed a third TLS phenotype, namely dense lymphocytic clusters containing B and T cells without any apparent FDC networks or GC (**Fig. 1H, I, Supplementary Fig. S2A**). All three TLS phenotypes shared a common localization near CXCL13$^+$ blood vessels (**Fig. 1F-I**, arrowheads, **Supplementary Fig. S2A-C,** arrowheads). Because CXCL13-expressing perivascular cells, B and T cells are essential for the development of TLS, we propose that clusters without FDC represent the first stage of TLS development and term these here as early TLS (E-TLS). In analogy to the stages of SLO follicles, we called FDC-containing TLS without GC as primary follicle-like TLS (PFL-TLS), and GC-containing TLS as secondary follicle-like TLS (SFL-TLS).

Because HEVs and mature DCs are often located within TLS and their numbers are associated with improved outcome of cancer patients(12,39), we analyzed whether these cell types were associated with any particular TLS maturation stage by using multiparameter IF. We detected DC-LAMP+ (DCs) and PNAD+ cells (HEVs) in TLS at all maturation stages with similar frequencies (**Fig. 1J**) as well as in lymphocyte-rich areas without apparent organization into TLS (**Fig. 1K**, right).

Tumor-associated TLS develop within a specialized microanatomical niche

To identify factors involved in the development of LSCC-associated TLSs we selected a set of patients with high and low TLS densities and investigated the expression of chemokine transcripts associated with lymphoid neogenesis in lung inflammation (3,37). We found a significantly higher expression of *CXCL13*, *LTB* and *CCL21* in TLS-high LSCCs (**Fig. 2A**). Due to high intergroup variability we did not detect a significant difference in the expression of CXCL12 between TLS-high and TLS-low patients. Nevertheless, we found a direct correlation between *CXCL12* expression and TLS density by Spearman correlation analysis (R=0.44, *p*=0.019), while *IL-17A*, *CCL19* and other previously published TLS-associated factors did not correlate (**Supplementary Table S5**).

We analyzed the expression of the relevant chemokines in LSCC tissues and found that CCL21 was expressed by HEVs within TLS, and CXCL13 by perivascular and TLS-associated stromal cells as well as by 75% of tumors (**Supplementary Fig. S3A)**. CXCL12, which is produced by alveolar and bronchial epithelium in steady state, was highly expressed by 90% of the tumors and by focal clusters of hyperplastic epithelial cells nearby TLS (**Supplementary Fig. S3A)**. Cells in such clusters also expressed variable amounts of PD-L1 and LTB (**Fig. 2B-D, Supplementary Fig. S3B)**. We observed such clusters in all patients with TLS in the alveolar compartment and independently of the TLS maturation stage (**Fig. 2D**). Taken together, lung parenchyma provides a favorable environment for TLS development, which involves CXCL13 production by perivascular and stromal cells, CCL21 production by HEVs as well as LTB, PD-L1 and CXCL12 production by hyperplastic alveolar epithelial cells.

The density of LSCC-associated TLS predicts survival and is associated with an adaptive immune response-related signature

To test the prognostic significance of TLS density in our cohort we defined a threshold for separating patients with high and low TLS densities by ROC curve analysis (**Fig. 3A**). In Kaplan-Meier analysis high TLS density (>0.165 TLS/mm^2) significantly correlated with improved progression-free (PFS), disease-free and overall survival (**Fig. 3B**). Among the significant covariates (**Table 1**) TLS density and tumor stage were the only two independent predictors of PFS in a multivariate Cox regression analysis (**Supplementary Table S6**). We confirmed the positive correlation between high TLS density and improved survival in

Author Manuscript Published OnlineFirst on December 26, 2017; DOI: 10.1158/0008-5472.CAN-17-1987
Author manuscripts have been peer reviewed and accepted for publication but have not yet been edited.

another, geographically distinct NSCLC patient cohort (**Supplementary Table S1**) by scoring TLS density in a single H&E image per patient (**Supplementary Fig. S4A**).

To understand the possible reasons of the prognostic benefit, we investigated whether TLS are associated with the immunological makeup of a tumor. We compared the expression of various immune response-related genes (**Supplementary Table S5**) in a set of TLS-high and TLS-low patients. The expression of transcripts related to adaptive immunity including *CD27*, *CD8A, IL-21, IGKC* and others (**Fig. 3C**) was significantly upregulated in TLS-high tumors or directly correlated with TLS density (**Supplementary Fig. S4B)**. Whereas the expression of innate response-related genes such as *NKP46* and *ITGAM* (encoding CD11b) was similar in both patient groups (**Supplementary Table S5**). The expression of most TLS-associated genes was prognostic forth improved PFS in an independent LSCC cohort (n=141) available from the online repository, Kaplan-Meier plotter (40) (**Supplementary Fig. S4C)**. Taken together, high TLS density is an independent positive prognostic marker for LSCC patients and suggests an increased intratumoral adaptive immune response.

Neoadjuvant chemotherapy impairs TLS maturation and abrogates the prognostic power of TLS

Histology analysis revealed a strong positive correlation between TLS density and the presence of GC (**Fig. 4A**), and a negative correlation between GC and the use of neoadjuvant chemotherapy (**Supplementary Table S7**). A significantly lower proportion of neoadjuvant chemotherapy-treated patients showed GC^+ TLS (**Fig. 4B**) compared to chemotherapy-naïve patients, while TLS density was similar (**Fig. 4C**). We performed an in-depth analysis of TLS maturation in different patients groups using multiparameter IF and quantitative pathology (**Fig. 4D**). We determined the number of TLS in each maturation stage and compared the proportion of each stage in patients with high and low TLS densities and in patients after neoadjuvant chemotherapy. TLS maturation significantly correlated with TLS density in

Author Manuscript Published OnlineFirst on December 26, 2017; DOI: 10.1158/0008-5472.CAN-17-1987
Author manuscripts have been peer reviewed and accepted for publication but have not yet been edited.

chemotherapy-naïve patients (Spearman R= 0.32, *p*=0.01), but not in chemotherapy-treated patients (Spearman R= -0.09, *p*=0.6) Specifically, TLS maturation was arrested at the E-TLS stage in TLS-low patients (**Fig. 4E**, left panel) resulting in a significantly reduced SFL-TLS proportion (**Fig. 4E**, right panel) and decreased GC size (**Fig. 4F**) when compared to TLS-high patients.

To determine the impact of neoadjuvant therapy on TLS maturation we analyzed only TLS-high patients and observed that the proportion of SFL-TLS (**Fig. 4G**) as well as GC size (**Fig. 4H**) was significantly reduced in patients after neoadjuvant radio- or chemotherapy. Because neoadjuvant chemotherapy is used for patients with advanced disease, we separately compared TLS maturation in chemotherapy-naïve patients with early- and late-stage disease. We observed that only early-stage patients had a significantly higher proportion of SFL-TLS than chemotherapy-treated patients, while GC size was significantly higher in both early- and late-stage chemotherapy-naïve patients (**Supplementary Fig. S5A, B**).

Because GC result from cognate interactions between T and B cells, their presence in TLS may point towards an ongoing immune response, which may be tumor-specific. We thus hypothesized that the reduction of GC in neoadjuvant chemotherapy-treated patients indicates dysfunctional TLS and abrogates the prognostic relevance of TLS density. Indeed, in neoadjuvant chemotherapy-treated patients TLS density had no prognostic power (**Fig. 4I**). In contrast, TLS density was an independent prognostic marker, stronger than tumor stage in chemotherapy-naïve patients (**Table 2**). To verify the prognostic relevance of TLS maturation in the absence of potential negative impact of chemotherapy we determined the association between the number of each TLS maturation stage determined in the IF images and the progression-free survival in chemotherapy-naïve patients. Only the number or the proportion of SFL-TLS significantly correlated with improved survival (**Supplementary Fig. S5C-E**). Taken together, these data show that neoadjuvant therapy impairs TLS maturation and reveal the essential role of GC for the prognostic power of TLS density in patients with LSCC.

Author Manuscript Published OnlineFirst on December 26, 2017; DOI: 10.1158/0008-5472.CAN-17-1987
Author manuscripts have been peer reviewed and accepted for publication but have not yet been edited.

Corticosteroids impair TLS development in the lungs

The cytotoxic effects of chemo- and radiotherapy may have a negative impact on the rapidly proliferating GC B cells thus leading to GC shrinkage; however, all patients receiving neoadjuvant therapy were also concomitantly treated with corticosteroids to manage side effects. Thus we hypothesized that the immunosuppressive properties of corticosteroids negatively influence TLS development. To investigate this possibility we compared TLS density and maturation in neoadjuvant therapy-naïve LSCC patients, who were treated with corticosteroids before resection because of non-cancer-related comorbidities (**Supplementary Table S4**) or who had not received corticosteroids. Tumors of corticosteroid-treated patients showed a significantly lower TLS density, reduced proportion of SFL-TLS as well as GC size (**Fig. 5A-C**), independently of whether steroids were given locally or systemically.

To provide direct experimental evidence for our observation that corticosteroids interfere with lung TLS development and/or maturation, we induced TLS in the lungs of mice by intranasal (i.n.) administration of alum with or without Ova as an antigen (adapted from (33)) and investigated the impact of systemic low-dose dexamethasone treatment (**Fig. 5D**). We characterized TLS maturation by multiparameter IF using B220, CD21/35 and PNA to stain B cells, FDC and GC, respectively. We observed that TLS development in response to i.n. alum followed the same maturation stages as in LSCC patients (**Fig. 5E**). However, the addition of Ova was necessary to induce high TLS density and GC formation (**Fig. 5F-G**). Systemic dexamethasone treatment did not significantly affect B cell, T cell and myeloid cell proportions in the spleen (**Fig. 5H**) and did not affect the density of TLS in the lungs (**Fig. 5G**) but significantly reduced the proportion of PFL- and SFL-TLS (**Fig. 5H**). Collectively, our data suggest that corticosteroids have a negative impact on TLS development in the lungs independently of cytotoxic therapies.

DISCUSSION

We performed a comprehensive analysis of LSCC tissues to study TLSs as whole microanatomical structures. Healthy human lungs are devoid of TLS (34), while most LSCC patients had peritumoral TLS in close vicinity to hyperplastic alveolar epithelial cells, which express CXCL12 and LTB. A fraction of these cells expressed considerable amounts of PD-L1 rather than chemokines. Cells with similar morphology are present next to TLS in infected human lungs (41) and in advanced-stage COPD patients where they generate an alveolar-lymphoid interface containing antigen-capturing DC (42). We propose that these cells support TLS development as we observed them close to TLS in all patients and at all TLS maturation stages. Our observation that the pleural wall, which lacks such cells, contained significantly less TLS than the alveolar compartment (**Fig. 1D**) supports this idea. However, direct experimental evidence is needed to verify this assumption. The morphology of this cell cluster resembles the dome-shaped lymphoepithelium (M cells) of the gut-associated TLS, which has a unique ability to transport antigens from the gut lumen to the underlying DC (43). M cell-like cells are present also in the respiratory tract of various animal species and deliver material from the airway lumen to DCs in the underlying lymphoid follicles (44,45). Whether the hyperplastic epithelial cells surrounding TLS in human lungs likewise participate in antigen delivery to TLS is currently unknown.

We showed that expression of CXCL13, LTB, CCL21 and CXCL12 correlates with TLS density in LSCC. In contrast, IL-17A and other chemokines relevant for iBALT formation in different lung inflammatory conditions (34) do not seem to be involved in the generation of LSCC-associated TLS. In the lungs, B cells are the main source of CXCL13 in response to cigarette smoke or LPS and are plausible drivers of TLS development in the lungs of COPD patients via Toll-like receptor and LTBR signaling (29). In LSCC, however, CXCL13 was mainly produced by TLS-associated perivascular and stromal cells and may serve as entry sites for lymphocytes from the blood stream. We thus propose that B cell and T cell clusters without differentiated FDCs near CXCL13$^+$ blood vessels represent the initial stage of TLS development. Various stimuli including IL-1 (46,47) and cigarette smoke (48) induce the production of CXCL13 in lung mesenchymal cells. However, the mechanisms driving the expression of CXCL13 by perivascular cells or the formation of the hyperplastic TLS-associated epithelium in LSCC are currently unknown.

In mice, naïve B cells respond to CXCL13 by producing LTB (49), which is crucial for the differentiation of FDCs from perivascular mesenchymal precursors and TLS development (36). We observed that hyperplastic epithelial cells and lymphocytes within early TLS produce LTB (**Fig. 2C**), which might drive the differentiation of FDC and generate the PFL-TLS in human lungs. The subsequent establishment of SFL-TLSs presumably requires antigen-dependent interactions between DCs, T cells and B cells. CCL21 is mainly expressed by HEVs and lymphatic vessels, and attracts DCs and T cells to the developing TLS in different tissues (7). Our data suggest an upstream function of DCs and HEVs in the development of TLS because they are already present in E-TLS as well as in lymphocyte rich areas without apparent organization. However, it is currently unclear if such areas are the initiation sites of TLS or how these cell types dictate the generation of a mature TLS. We observed that TLS development follows the same steps in CRC (50) and in the lungs of mice after i.n. administration of alum + Ova. Thus, the described TLS maturation sequence may represent a general mechanism of TLS development. A clear understanding of TLS dynamics in the tumor microenvironment is currently lacking. It has been shown in the context of viral lung infection that TLS persist in lungs for at least 4 weeks after the clearance of the virus (4), however, it is unclear whether each single TLS was maintained for at least 4 weeks or whether TLS developed and disappeared at a certain rate during these 4 weeks. Tumor models with synchronized TLS development could be used to address this question; targeting of

Author Manuscript Published OnlineFirst on December 26, 2017; DOI: 10.1158/0008-5472.CAN-17-1987
Author manuscripts have been peer reviewed and accepted for publication but have not yet been edited.

LIGHT to tumor vasculature (24) may represent such a model, although it is currently unknown whether GC develop in this setting.

We identified TLS density as the most significant and independent prognostic marker in untreated LSCC patients, which even outperformed tumor stage. Because TLS often correlate with increased lymphocytic infiltrate that has a pronounced prognostic benefit on its own (8), the causal relationship between TLS and lymphocytic infiltrate is unclear. Here we demonstrate that TLS and not the diffuse infiltration of lymphocytes or plasma cells is an independent prognostic factor for progression free survival (**Table 2, Supplementary Table S6**), suggesting that at least in LSCC, the structural organization of lymphocytes is the confounding factor for prognosis.

TLS density can be assessed in diagnostic H&E sections and can thus be easily introduced in routine pathology to serve as a relevant prognostic parameter. Neoadjuvant chemotherapy-treated patients, however, showed similar TLS density but significantly less and smaller GC when compared to untreated patients. Due to the lack of paired pre- and post-therapy samples we cannot exclude that neoadjuvant chemotherapy-treated patients had a reduced TLS maturation already before the therapy. Nevertheless, we did observe a significant reduction in GC size when compared to stage-matched chemotherapy-naïve patients (**Supplementary Fig. S5B**). In mice, *de novo* formation of B cell follicles and the growth of GC size is crucial for an effective immune response (51). We thus propose that the low frequency and reduced size of GC in tumor-associated TLS after neoadjuvant chemotherapy reflects impaired TLS function. This is in line with the observation that the prognostic power of TLS density was lost in these patients. Further, we demonstrate that only SFL-TLS but not E-TLS or PFL-TLS correlated with improved survival in chemotherapy-naïve patients. The notion that the presence of GC reflects the function of TLS in anti-tumor immunity is also supported by Posch et al. showing that the integration of TLS maturation and TLS density into a joint TLS immunoscore had a superior predictive power for the recurrence risk in untreated non-

Author Manuscript Published OnlineFirst on December 26, 2017; DOI: 10.1158/0008-5472.CAN-17-1987
Author manuscripts have been peer reviewed and accepted for publication but have not yet been edited.

metastatic CRC than TLS density alone (50). However, direct evidence for the presence and activation of tumor-specific B and/or T cells in cancer-associated TLS is still lacking.

We propose that corticosteroids are at least partly responsible for the impaired TLS development in the neoadjuvant chemotherapy-treated LSCC patients for the following reasons. First, we observed a significantly lower TLS density and reduced GC formation in LSCC patients who were treated with corticosteroids but did not receive neoadjuvant chemotherapy. Second, we observed that dexamethasone significantly decreased the development of alum + Ova-induced mature TLS in the lungs of mice. Third, corticosteroid-treated COPD patients have a significantly reduced TLS density in comparison to COPD patients who did not receive corticosteroids (52). Finally, corticosteroid treatment abolishes the formation of GC in BALT in experimental rat pulmonary granuloma (53). A possible explanation is offered by a study demonstrating that prednisolone induces apoptosis of human GC B cells by blocking both surface immunoglobulin- and CD40-mediated survival pathways (54). Despite the concomitant use of corticosteroids, the TLS density in chemotherapy-treated patients was not diminished. We propose that chemotherapy-induced inflammation in the tumor microenvironment (55) overrides the negative impact of steroids on TLS initiation (reflected by total TLS density), but is not sufficient to override the negative impact on GC maturation (reflected by proportion of SFL-TLS). Similarly, in the lungs of mice receiving proinflammatory alum i.n., steroid treatment did not decrease TLS density (**Fig. 5F**) whereas it reduced TLS maturation (**Fig. 5G**). Our findings indicate that corticosteroid treatment of cancer patients may not only decrease their spontaneous immune defense to cancer but also suppress the response to immunotherapy as well as to treatments that induce immunogenic cell death such as radiotherapy (56) and chemotherapy (57). Thus the use of alternative non-steroid drugs for managing adverse effects of chemo-, radio- or immune therapy should be considered.

In summary, the work presented here extends the current knowledge by (1) characterizing the niche that fosters TLS development in the lungs, (2) determining stages of TLS maturation that affect the prognostic relevance of TLS density, and (3) discovering the negative impact of corticosteroids on TLS development in LSCC that is associated with poor outcome in chemotherapy-naïve patients.

ACKNOWLEDGEMENTS

We thank Stefanie Hiltbrunner and Paulino Tallon de Lara (Institute of Experimental Immunology, University of Zurich) for critical reading of the manuscript and helpful discussions, Mathias Heikenwaelder (Helmholtz Zentrum Munich, Germany) for providing the anti-LTB antibody, and the personnel of the Laboratory Animal Services Center (University of Zurich) for expert animal care.

This work was financially supported by the Swiss National Science Foundation (SNSF, 31003A_152851, MvdB), the Sciex Foundation (13.046, MvdB, KS, AL), the Science Foundation for Oncology (MvdB), the Cancer League Zurich (KLZ_2015_vandenBroek, MvdB, KS), the Novartis Research Foundation (15B096, KS), the University Research Priority Program "Translational Cancer Research" (MvdB, KS), Swiss Cancer League (AS), SNSF SystemsX (AS) and the Latvian National Research Program "Biomedicine" (AL).

REFERENCES

1. Neyt K, Perros F, GeurtsvanKessel CH, Hammad H, Lambrecht BN. Tertiary lymphoid organs in infection and autoimmunity. Trends in immunology **2012**;33:297-305
2. Dieu-Nosjean MC, Giraldo NA, Kaplon H, Germain C, Fridman WH, Sautes-Fridman C. Tertiary lymphoid structures, drivers of the anti-tumor responses in human cancers. Immunological reviews **2016**;271:260-75
3. Silina K, Rulle U, Kalnina Z, Line A. Manipulation of tumour-infiltrating B cells and tertiary lymphoid structures: a novel anti-cancer treatment avenue? Cancer immunology, immunotherapy : CII **2014**;63:643-62
4. Halle S, Dujardin HC, Bakocevic N, Fleige H, Danzer H, Willenzon S*, et al.* Induced bronchus-associated lymphoid tissue serves as a general priming site for T cells and is maintained by dendritic cells. The Journal of experimental medicine **2009**;206:2593-601
5. Moyron-Quiroz JE, Rangel-Moreno J, Kusser K, Hartson L, Sprague F, Goodrich S*, et al.* Role of inducible bronchus associated lymphoid tissue (iBALT) in respiratory immunity. Nature medicine **2004**;10:927-34
6. Wada Y, Nakashima O, Kutami R, Yamamoto O, Kojiro M. Clinicopathological study on hepatocellular carcinoma with lymphocytic infiltration. Hepatology **1998**;27:407-14
7. Hiraoka N, Ino Y, Yamazaki-Itoh R. Tertiary Lymphoid Organs in Cancer Tissues. Frontiers in immunology **2016**;7:244
8. Fridman WH, Zitvogel L, Sautes-Fridman C, Kroemer G. The immune contexture in cancer prognosis and treatment. Nature reviews Clinical oncology **2017**

9. Garnelo M, Tan A, Her Z, Yeong J, Lim CJ, Chen J, *et al.* Interaction between tumour-infiltrating B cells and T cells controls the progression of hepatocellular carcinoma. Gut **2015**

10. Knief J, Reddemann K, Petrova E, Herhahn T, Wellner U, Thorns C. High Density of Tumor-infiltrating B-Lymphocytes and Plasma Cells Signifies Prolonged Overall Survival in Adenocarcinoma of the Esophagogastric Junction. Anticancer research **2016**;36:5339-45

11. Dieu-Nosjean MC, Antoine M, Danel C, Heudes D, Wislez M, Poulot V, *et al.* Long-term survival for patients with non-small-cell lung cancer with intratumoral lymphoid structures. Journal of clinical oncology : official journal of the American Society of Clinical Oncology **2008**;26:4410-7

12. Goc J, Germain C, Vo-Bourgais TK, Lupo A, Klein C, Knockaert S, *et al.* Dendritic cells in tumor-associated tertiary lymphoid structures signal a Th1 cytotoxic immune contexture and license the positive prognostic value of infiltrating CD8+ T cells. Cancer research **2014**;74:705-15

13. Germain C, Gnjatic S, Tamzalit F, Knockaert S, Remark R, Goc J, *et al.* Presence of B cells in tertiary lymphoid structures is associated with a protective immunity in patients with lung cancer. American journal of respiratory and critical care medicine **2014**;189:832-44

14. de Chaisemartin L, Goc J, Damotte D, Validire P, Magdeleinat P, Alifano M, *et al.* Characterization of chemokines and adhesion molecules associated with T cell presence in tertiary lymphoid structures in human lung cancer. Cancer research **2011**;71:6391-9

15. Kroeger DR, Milne K, Nelson BH. Tumor-Infiltrating Plasma Cells Are Associated with Tertiary Lymphoid Structures, Cytolytic T-Cell Responses, and Superior

Prognosis in Ovarian Cancer. Clinical cancer research : an official journal of the American Association for Cancer Research **2016**;22:3005-15

16. Goc J, Germain C, Vo-Bourgais TK, Lupo A, Klein C, Knockaert S, *et al.* Dendritic cells in tumor-associated tertiary lymphoid structures license the positive prognostic value of tumor-infiltrating CD8+ T cells. Cancer research **2013**

17. Nzula S, Going JJ, Stott DI. Antigen-driven clonal proliferation, somatic hypermutation, and selection of B lymphocytes infiltrating human ductal breast carcinomas. Cancer research **2003**;63:3275-80

18. Coronella JA, Spier C, Welch M, Trevor KT, Stopeck AT, Villar H, *et al.* Antigen-driven oligoclonal expansion of tumor-infiltrating B cells in infiltrating ductal carcinoma of the breast. Journal of immunology **2002**;169:1829-36

19. Zhu W, Germain C, Liu Z, Sebastian Y, Devi P, Knockaert S, *et al.* A high density of tertiary lymphoid structure B cells in lung tumors is associated with increased CD4+ T cell receptor repertoire clonality. Oncoimmunology **2015**;4:e1051922

20. van de Pavert SA, Mebius RE. New insights into the development of lymphoid tissues. Nature reviews Immunology **2010**;10:664-74

21. Luther SA, Lopez T, Bai W, Hanahan D, Cyster JG. BLC expression in pancreatic islets causes B cell recruitment and lymphotoxin-dependent lymphoid neogenesis. Immunity **2000**;12:471-81

22. Bindea G, Mlecnik B, Tosolini M, Kirilovsky A, Waldner M, Obenauf AC, *et al.* Spatiotemporal dynamics of intratumoral immune cells reveal the immune landscape in human cancer. Immunity **2013**;39:782-95

23. Schrama D, Voigt H, Eggert AO, Xiang R, Zhou H, Schumacher TN, *et al.* Immunological tumor destruction in a murine melanoma model by targeted LTalpha independent of secondary lymphoid tissue. Cancer immunology, immunotherapy : CII **2008**;57:85-95

24. Johansson-Percival A, He B, Li ZJ, Kjellen A, Russell K, Li J, *et al.* De novo induction of intratumoral lymphoid structures and vessel normalization enhances immunotherapy in resistant tumors. Nature immunology **2017**

25. Lutz ER, Wu AA, Bigelow E, Sharma R, Mo G, Soares K, *et al.* Immunotherapy converts nonimmunogenic pancreatic tumors into immunogenic foci of immune regulation. Cancer immunology research **2014**;2:616-31

26. Fleige H, Ravens S, Moschovakis GL, Bolter J, Willenzon S, Sutter G, *et al.* IL-17-induced CXCL12 recruits B cells and induces follicle formation in BALT in the absence of differentiated FDCs. The Journal of experimental medicine **2014**;211:643-51

27. Luther SA, Bidgol A, Hargreaves DC, Schmidt A, Xu Y, Paniyadi J, *et al.* Differing activities of homeostatic chemokines CCL19, CCL21, and CXCL12 in lymphocyte and dendritic cell recruitment and lymphoid neogenesis. Journal of immunology **2002**;169:424-33

28. Hasday JD, Bascom R, Costa JJ, Fitzgerald T, Dubin W. Bacterial endotoxin is an active component of cigarette smoke. Chest **1999**;115:829-35

29. Litsiou E, Semitekolou M, Galani IE, Morianos I, Tsoutsa A, Kara P, *et al.* CXCL13 production in B cells via Toll-like receptor/lymphotoxin receptor signaling is involved in lymphoid neogenesis in chronic obstructive pulmonary disease. American journal of respiratory and critical care medicine **2013**;187:1194-202

30. Roos AB, Sanden C, Mori M, Bjermer L, Stampfli MR, Erjefalt JS. IL-17A Is Elevated in End-Stage Chronic Obstructive Pulmonary Disease and Contributes to Cigarette Smoke-induced Lymphoid Neogenesis. American journal of respiratory and critical care medicine **2015**;191:1232-41

31. Nikota JK, Shen P, Morissette MC, Fernandes K, Roos A, Chu DK, *et al.* Cigarette smoke primes the pulmonary environment to IL-1alpha/CXCR-2-dependent

nontypeable Haemophilus influenzae-exacerbated neutrophilia in mice. Journal of immunology **2014**;193:3134-45

32. Morissette MC, Jobse BN, Thayaparan D, Nikota JK, Shen P, Labiris NR*, et al.* Persistence of pulmonary tertiary lymphoid tissues and anti-nuclear antibodies following cessation of cigarette smoke exposure. Respir Res **2014**;15:49

33. Kuroda E, Ozasa K, Temizoz B, Ohata K, Koo CX, Kanuma T*, et al.* Inhaled Fine Particles Induce Alveolar Macrophage Death and Interleukin-1alpha Release to Promote Inducible Bronchus-Associated Lymphoid Tissue Formation. Immunity **2016**;45:1299-310

34. Hwang JY, Randall TD, Silva-Sanchez A. Inducible Bronchus-Associated Lymphoid Tissue: Taming Inflammation in the Lung. Frontiers in immunology **2016**;7:258

35. Jones GW, Hill DG, Jones SA. Understanding Immune Cells in Tertiary Lymphoid Organ Development: It Is All Starting to Come Together. Frontiers in immunology **2016**;7:401

36. Krautler NJ, Kana V, Kranich J, Tian Y, Perera D, Lemm D*, et al.* Follicular dendritic cells emerge from ubiquitous perivascular precursors. Cell **2012**;150:194-206

37. Goc J, Fridman WH, Sautes-Fridman C, Dieu-Nosjean MC. Characteristics of tertiary lymphoid structures in primary cancers. Oncoimmunology **2013**;2:e26836

38. Bustin SA, Benes V, Garson JA, Hellemans J, Huggett J, Kubista M*, et al.* The MIQE guidelines: minimum information for publication of quantitative real-time PCR experiments. Clinical chemistry **2009**;55:611-22

39. Martinet L, Filleron T, Le Guellec S, Rochaix P, Garrido I, Girard JP. High endothelial venule blood vessels for tumor-infiltrating lymphocytes are associated with lymphotoxin beta-producing dendritic cells in human breast cancer. Journal of immunology **2013**;191:2001-8

40. Szasz AM, Lanczky A, Nagy A, Forster S, Hark K, Green JE, *et al.* Cross-validation of survival associated biomarkers in gastric cancer using transcriptomic data of 1,065 patients. Oncotarget **2016**

41. Tschernig T, Pabst R. Bronchus-associated lymphoid tissue (BALT) is not present in the normal adult lung but in different diseases. Pathobiology **2000**;68:1-8

42. Mori M, Andersson CK, Svedberg KA, Glader P, Bergqvist A, Shikhagaie M, *et al.* Appearance of remodelled and dendritic cell-rich alveolar-lymphoid interfaces provides a structural basis for increased alveolar antigen uptake in chronic obstructive pulmonary disease. Thorax **2013**;68:521-31

43. Randall TD. Bronchus-associated lymphoid tissue (BALT) structure and function. Adv Immunol **2010**;107:187-241

44. Wang M, Gao Z, Zhang Z, Pan L, Zhang Y. Roles of M cells in infection and mucosal vaccines. Hum Vaccin Immunother **2014**;10:3544-51

45. Pabst R, Tschernig T. Bronchus-associated lymphoid tissue: an entry site for antigens for successful mucosal vaccinations? Am J Respir Cell Mol Biol **2010**;43:137-41

46. Lisignoli G, Cristino S, Toneguzzi S, Grassi F, Piacentini A, Cavallo C, *et al.* IL1beta and TNFalpha differently modulate CXCL13 chemokine in stromal cells and osteoblasts isolated from osteoarthritis patients: evidence of changes associated to cell maturation. Exp Gerontol **2004**;39:659-65

47. Neyt K, GeurtsvanKessel CH, Deswarte K, Hammad H, Lambrecht BN. Early IL-1 Signaling Promotes iBALT Induction after Influenza Virus Infection. Frontiers in immunology **2016**;7:312

48. Bracke KR, Verhamme FM, Seys LJ, Bantsimba-Malanda C, Cunoosamy DM, Herbst R, *et al.* Role of CXCL13 in cigarette smoke-induced lymphoid follicle formation and chronic obstructive pulmonary disease. American journal of respiratory and critical care medicine **2013**;188:343-55

49. Ansel KM, Ngo VN, Hyman PL, Luther SA, Forster R, Sedgwick JD*, et al.* A chemokine-driven positive feedback loop organizes lymphoid follicles. Nature **2000**;406:309-14

50. Posch F, Silina K, Leibl S, Mündlein A, Moch H, Siebenhüner A*, et al.* Maturation of tertiary lymphoid structures predicts the risk for recurrence in stage II and III colorectal cancer. Oncoimmunology **2017**;Accepted

51. Dubey LK, Lebon L, Mosconi I, Yang CY, Scandella E, Ludewig B*, et al.* Lymphotoxin-Dependent B Cell-FRC Crosstalk Promotes De Novo Follicle Formation and Antibody Production following Intestinal Helminth Infection. Cell Rep **2016**;15:1527-41

52. Hogg JC, Chu FS, Tan WC, Sin DD, Patel SA, Pare PD*, et al.* Survival after lung volume reduction in chronic obstructive pulmonary disease: insights from small airway pathology. American journal of respiratory and critical care medicine **2007**;176:454-9

53. Gemma H, Sato A. [Effect of glucocorticoid on lung tissue and bronchus-associated lymphoid tissue of experimental granulomatous lung]. Kekkaku **1989**;64:387-99

54. Holder MJ, Knox K, Gordon J. Factors modifying survival pathways of germinal center B cells. Glucocorticoids and transforming growth factor-beta, but not cyclosporin A or anti-CD19, block surface immunoglobulin-mediated rescue from apoptosis. European journal of immunology **1992**;22:2725-8

55. Apetoh L, Ghiringhelli F, Tesniere A, Obeid M, Ortiz C, Criollo A*, et al.* Toll-like receptor 4-dependent contribution of the immune system to anticancer chemotherapy and radiotherapy. Nature medicine **2007**;13:1050-9

56. Surace L, Lysenko V, Fontana AO, Cecconi V, Janssen H, Bicvic A*, et al.* Complement is a central mediator of radiotherapy-induced tumor-specific immunity and clinical response. Immunity **2015**;42:767-77

Author Manuscript Published OnlineFirst on December 26, 2017; DOI: 10.1158/0008-5472.CAN-17-1987
Author manuscripts have been peer reviewed and accepted for publication but have not yet been edited.

57. Galluzzi L, Buque A, Kepp O, Zitvogel L, Kroemer G. Immunological Effects of Conventional Chemotherapy and Targeted Anticancer Agents. Cancer Cell **2015**;28:690-714

Author Manuscript Published OnlineFirst on December 26, 2017; DOI: 10.1158/0008-5472.CAN-17-1987
Author manuscripts have been peer reviewed and accepted for publication but have not yet been edited.

TABLES

Table 1. Clinical and histological characteristics of the LSCC patient cohort (n=138) from the University Hospital Zurich

Characteristics	Number	%	Median PFS	HR[a] (CI 95%)
Gender Male	111	80.4	827	1.1
Female	27	19.6	1060	(0.6-2.1)
Age (Mean±SEM 63±0.8)				1
< Median	60	43.5	894	(0.97-1)
= Median (62)	12	8.7	1236	
> Median	66	47.8	796	
Smoking history				0.9
Current	79	57.2	1172	(0.7-1.8)
Former	59	42.8	555	
Pack-years (Mean±SEM 52±2)				1
< Median	56	40.6	533	(0.99-1)
= Median (50)	22	15.9	1539	
> Median	56	40.6	916	
ND	4	2.9	1187	
pT/ypT 0	7	5.1	1434	1.3***
1a	26	18.8	1390	(1.1-1.5)
1b	13	9.4	2167	
2a	27	19.6	1123	
2b	11	8.0	1055	
3	31	22.5	652	
4	23	16.7	360	
pN 0	62	44.9	1394	1.7**
1	48	34.8	761	(1.2-2.3)
2	28	20.3	418	
pM 0	132	95.7	1058	7.3***
1a	3	2.2	180	(2.9-18)
1b	3	2.2	2	
Stage 0	6	4.3	1518	1.4***
1a	22	15.9	1678	(1.2-1.7)
1b	10	7.2	1073	
2a	29	21.0	1283	
2b	16	11.6	797	
3a	43	31.2	414	
3b	8	5.8	512	
4	4	2.9	91	
Neoadjuvant chemotherapy[b]				1
Yes	51	37.0	495	(0.62-1.7)
No	87	63.0	1060	

Characteristics	Number	%	Median PFS	HR[a] (CI 95%)
Grade 2	61	44.2	1060	1.1
3	77	55.8	725	(0.55-1.83)
Tumor Size (Mean±SEM 4.3±0.2)				1.2***
< Median	67	48.6	1471	(1.1-1.3)
= Median (3.8)	4	2.9	415	
> Median	67	48.6	451	
Pleural Invasion				1.5
Yes	41	29.7	509	(0.92-2.5)
No	97	70.3	1123	
Vascular Invasion				1.6
Yes	55	39.9	414	(0.97-2.6)
No	83	60.1	1146	
Adjuvant therapy[c]				1.9**
Chemotherapy	23	16.7	509	(1.3-2.8)
Radiotherapy	16	11.6	339	
Chemo+Radio	5	3.6	414	
None	94	68.1	1162	
Corticosteroid treatment[d]				1.2
Local	12	8.7	627	(0.74-2)
Systemic	57	41.3	495	
None	63	45.7	1172	
ND	6	4.3	720	
TLS density[e]				0.4**
TLS-low	47	34.1	451	(0.26-0.71)
TLS-high	91	65.9	1381	
GC formation[f]				0.6
No	53	38.4	495	(0.39-1)
Yes	85	61.6	1123	
TIL score (Mean±SEM 4.1±0.1)				0.75*
< Median	47	34.1	461	(0.6-0.93)
= Median (4)	21	15.2	410	
> Median	57	41.3	1178	
ND	13	9.4	1511	
Plasma cell score (Mean±SEM 3.2±0.2)				0.81*
< Median	56	40.6	465	(0.7-0.94)
= Median (3.5)	9	6.5	1055	
> Median	60	43.5	1426	
ND	13	9.4	1511	

PFS, progression-free survival; HR, hazard ratio; TLS, tertiary lymphoid structures; GC, germinal centers; ND, not determined.

TNM was assessed according to the 7th Edition of the TNM Staging System for non-small cell lung cancer.

[a] HR was calculated by the univariate Cox regression analysis for PFS comparing no vs. yes or low vs. high groups in case of categorical variables (pleural invasion, vascular invasion, neoadjuvant and adjuvant chemotherapy, steroid treatment, GC formation, TLS density) or comparing low to increasing values for continuous variables (age, pack years, pT, pN, pM, stage, grade, size). *P*-values according to Wald-test: *<0.05, **<0.005, ***<0.0005. Patients that had died sooner than 1 month after surgery were excluded from this analysis (n=6).

[b] For neoadjuvant chemotherapy platinols were used in combination with either gemcitabine (n=19) or taxols (n=27) or others (n=5).

[c] HR was calculated for all neoadjuvant chemotherapy-treated patients vs. untreated patients.

[d] Treatment of corticosteroids was considered if applied up to one month before surgery. All neoadjuvant chemotherapy-treated patients received systemic corticosteroids. Eighteen chemotherapy-naïve patients received corticosteroids because of cancer non-related comorbidities either systemically or locally (inhalation). HR was calculated for all steroid-treated vs. untreated patients.

[e] TLS density was measured as the number of TLS per mm^2 in the tumor periphery and defined as high if >0.165 TLS/mm^2.

[f] A tumor was considered GC-positive if at least one TLS showed the characteristic morphology of proliferating centroblasts.

Table 2. Multivariate Cox regression analysis of progression-free survival of neoadjuvant chemotherapy-naïve patients (n=85)

Variables in the equation	*p*-value	Hazard Ratio	95% CI Lower	95% CI Upper
Model 1[a]				
Stage[b]	0.007	1.38	1.1	1.73
Adjuvant therapy[c]	0.95	1	0.61	1.69
TLS density[c]	0.0003	0.28	0.14	0.56
TIL score[b]	0.5	0.88	0.61	1.28
Plasma cell score[b]	0.84	0.97	0.75	1.27
Model 2[a]				
Stage[c]	0.006	2.7	1.33	5.43
Adjuvant therapy[c]	0.94	1	0.61	1.72
TLS density[c]	0.0002	0.26	0.13	0.52
TIL score[b]	0.35	0.84	0.59	1.21
Plasma cell score[b]	0.96	1	0.77	1.32
Model 3[a]				
pT/ypT[b]	0.011	1.32	1.1	1.63
pN[b]	0.59	1.13	0.72	1.8
pM[b]	0.11	4.2	0.73	24
Adjuvant therapy[c]	0.66	1.13	0.65	1.95
TLS density[c]	0.002	0.34	0.17	0.67
TIL score[b]	0.29	0.82	0.56	1.19
Plasma cell score[b]	0.87	0.98	0.74	1.29

[A] Stage was analyzed either as a continuous variable (lower to higher) or as a categorical variable (early stage (0-2a) vs. late stage (3a-4)) in separate models. Because stage is dependent on TNM parameters we analysed these in a separate model.

[B] Continuous variables (smaller to larger)

[C] Categorical variables (no vs. yes or low vs high)

FIGURE LEGENDS

Figure 1. Development of LSCC-associated TLS. (**A**) A representative image of H&E-stained LSCC showing TLS in the adjacent normal tissue (N) in close proximity to the invasive front (white dashed line) of the tumor (T). GC in TLS were identified by a lighter central area (arrowheads, and left zoomed-in segment). Scale bar 500 μm. (**B, C**) The number of dense lymphocytic aggregates was determined in peritumoral lung parenchyma (**B**), and intratumoral regions (**C**) in 138 LSCC patients. The number of TLS per mm^2 defined the TLS density for each patient. (**D**) TLS density was compared in broncho-alveolar tissue (n=138) and pleura where possible (n=14) by 2-tailed Wilcoxon rank-sum test. (**E**) The structure and phenotype of GC-containing TLS was analysed in serial FFPE LSCC tissues from 5 patients with high TLS density by IHC. Scale bar 100 μm (**F-H**) IF staining for FDCs (CD21), GC cells (CD23) and CXCL13 was performed on serial sections spanning a depth of 250 μm of 2 LSCC patients with high TLS density. Slides were imaged using the multispectral microscopy system Vectra 3.0 (PerkinElmer). Each TLS was evaluated through the different depths and the images showing the widest TLS diameter (the central part) are shown. SFL-TLS, secondary follicle-like TLS with a GC reaction (white circle); PFL-TLS, primary follicle-like TLS with differentiated FDCs (white circle); E-TLS, early TLS. Arrowheads indicate the TLS-associated $CXCL13^+$ blood vessel. See also **Supplementary Fig. S2**. (**I**) IF staining for T cells (CD3), B cells (CD20) and CXCL13 was performed for 5 LSCC patients with high TLS density. Slides were imaged by AxioScan (Zeiss). A representative image showing dense lymphocytic cluster forming around a $CXCL13^+$ blood vessel (arrowhead) is shown. Scale bars 100 μm. (**J-K**) IF staining for FDCs (CD21), GC cells (CD23), B cells (CD20), DCs (DC-LAMP) and HEVs (PNAD) was performed on sections from 5 LSCC patients with high TLS density. (**J**) The number of TLS positive for HEVs and DCs was determined and compared in each TLS maturation stage. (**K**) Representative images of TLS in each

Author Manuscript Published OnlineFirst on December 26, 2017; DOI: 10.1158/0008-5472.CAN-17-1987
Author manuscripts have been peer reviewed and accepted for publication but have not yet been edited.

maturation stage and non-organized lymphocytic infiltrate containing DCs (white arrowheads) HEVs (magenta arrowheads) and DC-LAMP expressing lung epithelial cells (cyan arrowheads) are shown.

Figure 2. A specialized niche supports TLS development. (**A**) qRT-PCR analysis for transcripts of genes involved in lymphoid neogenesis was performed for chemotherapy-naïve patients with TLS-low (n=10) and TLS-high tumors (n=17)**.** Relative expression ($2^{\mathrm{Ct(cohort\ mean)-Ct(target\ gene)}}$) was normalized against the normalization factor (NF) calculated using three most stable reference genes in the selected cohort. Groups were statistically compared using the 2-tailed Wilcoxon rank-sum test with Benjamini and Hochberg correction for multiple testing. (**B-D**) Multiparameter-IF was performed in 5 LSCC patients with high TLS density for CXCL12, LTB, PD-L1 and cell type markers CDH1 (E-cadherin), CD45, CD21, and CD23. Representative images of hyperplastic TLS-associated epithelium are shown. Slides were imaged using a laser scanning confocal microscope (Leica) (**B, C**) or the Vectra imaging system (**D**). Scale bar 50 μm. See also **Supplementary Fig. S3.**

Figure 3. TLS density correlates with improved survival and adaptive immune response. (**A, B**) TLSs were quantified in H&E sections as described in **Fig. 1**. (**A**) ROC curve analysis was performed on chemotherapy-naïve patients with complete 3 year follow-up data (n=79) and identified 0.165 TLS/mm^2 as a threshold for separating TLS-high and TLS-low tumors with prognostic relevance. AUC, area under the curve. (**B**) Survival was compared for patients with high (>0.165 TLS/mm^2) and low TLS density by Kaplan-Meier curves. Confidence intervals are indicated as shaded areas surrounding survival curves. Significance was calculated by log-rank test. Patient numbers per group are indicated in brackets and numbers at risk are displayed for each 1000 days of follow-up. (**C**) qRT-PCR analysis for immune response-related transcripts was performed as described in **Fig. 2**. Groups were

Author Manuscript Published OnlineFirst on December 26, 2017; DOI: 10.1158/0008-5472.CAN-17-1987
Author manuscripts have been peer reviewed and accepted for publication but have not yet been edited.

compared using the 2-tailed Wilcoxon rank-sum test with Benjamini and Hochberg correction for multiple testing. See also **Supplementary Fig. S4**.

Figure 4. The prognostic value of TLS density is abrogated after neoadjuvant chemotherapy due to impaired GC formation. (**A**) TLS density was analyzed in H&E sections as described in **Fig. 1B**. A tumor was considered GC-positive if at least one TLS showed the characteristic morphology of proliferating centroblasts. TLS density was compared in patients with apparent GC (n=85, GC+) vs. no GC (n=53, GC-) by 2-tailed Wilcoxon rank-sum test. (**B**) The proportion of patients with GC^+ TLS in TLS-high patients with (n=37) or without (n=55) neoadjuvant chemotherapy (-/+ NeoCh), and TLS-low patients with (n=14) and without (n=34) neoadjuvant chemotherapy. $\chi 2$ test with Yates' correction was used to compare the proportion of patients with GC^+ TLS in +NeoCh and -NeoCh groups (p=0.012). (**C**) TLS density was compared in chemotherapy-naïve patients (-NeoCh, n=87) and -treated patients (+NeoCh, n=51) by 2-tailed Wilcoxon rank-sum test. (**D**) Quantitative pathology approach: IF was performed for B cells (CD20), T cells (CD3) and epithelial cells (panCK) (top row) or FDCs (CD21), GCs (CD23) and CXCL13 (middle row). To analyze TLS maturation stages and GC size tissue segmentation algorithm was trained to recognize dense DAPI cell clusters as lymphocytic aggregates, $CD21^+$ areas as FDC and $CD21^+CD23^+$ areas as GC (bottom row). The number of TLS in each maturation stage was determined and expressed as the proportion of all TLS for each patient. GC size was measured as the average number of pixels per GC area in each patient. (**E, F**) TLS maturation and GC size compared in chemotherapy-naïve patients with high (n=37) or low TLS density (n=24) by 2-tailed Wilcoxon rank-sum test. (**G, H**) TLS maturation and GC size were compared in TLS-high chemotherapy-naïve (-, n=37), neoadjuvant chemotherapy-treated (+Ch, n=28) or radiotherapy-treated (+RT, n=4) patients by 2-tailed Wilcoxon rank-sum test. The same significant differences were detected by the Kruskal-Wallis test with Dunn's multiple

comparison test comparing naïve vs. +Ch and naïve vs +RT groups. (**I**) Patients were stratified by neoadjuvant chemotherapy treatment and progression-free survival was compared in patients with high and low TLS density as described in **Fig. 3**. Patient numbers per group are indicated in brackets and numbers at risk are displayed for each 1000 days of follow-up.

Figure 5. TLS maturation is hampered by corticosteroids. (**A**) TLS density was analyzed in H&E-stained sections as described in **Fig. 1**. TLS density was compared in chemotherapy-naïve patients with no history of steroid treatment (n=63) and patients who received steroids until at least one month before surgery (n=18) by 2-tailed Wilcoxon rank-sum test. (**B, C**) TLS maturation and GC size were compared in a selection of chemotherapy-naïve patients as described in **Fig. 4**. Steroid-treated patients (n=15) were compared to untreated patients (n=43) by 2-tailed Wilcoxon rank-sum test. (**D**) Experimental design for TLS induction by i.n. administration of alum (200 µg/mouse) and ovalbumin (Ova, 50 µg/mouse) (adapted from (33)) and dexamethasone treatment (0.3 mg/kg). (**E**) Representative images of mouse lungs stained by IF to visualize different TLS maturation stages. Slides were imaged by Vectra 3.0. Scale bars 100 µm. (**F**) TLS density was determined as the number of dense B cell aggregates per lung lobe and compared in mice after TLS induction and dexamethasone treatment by one-way ANOVA and Dunnett's multiple comparison test. (**G**) TLS maturation stages were analyzed as described in **Fig. 4** with CD21/35^{+} areas recognized as FDCs and CD21/35^{+}PNA^{+} areas recognized as GCs; PNA also stains alveolar epithelium. (**H**) Spleens were collected at the time of sacrifice (**Fig. 5D**) and analyzed by flow cytometry. The following gates were applied prior to gating on the target populations: singlets/live cells/CD45^{+}. The proportions of B cells (B220^{+}), T cells (TCRβ^{+}) and myeloid cells (CD11b^{+}) from live cells is indicated. (**F-H**) Different treatment groups were compared by one-way ANOVA and Dunnett's multiple comparison test.

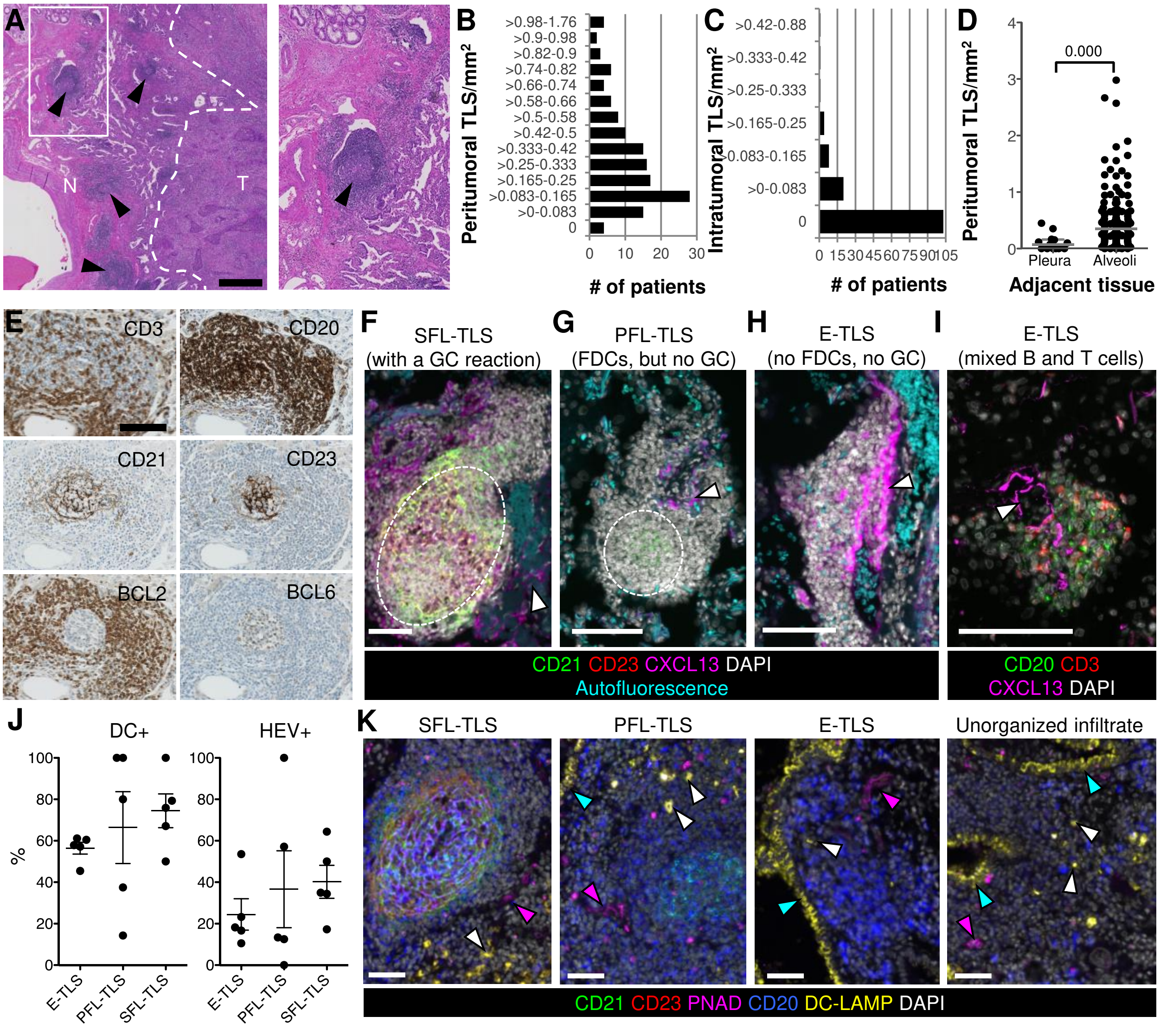
A
N
T
B
Peritumoral TLS/mm²
# of patients
C
Intratumoral TLS/mm²
# of patients
D
Peritumoral TLS/mm²
0.000
Pleura
Alveoli
Adjacent tissue
E
CD3
CD20
CD21
CD23
BCL2
BCL6
F
SFL-TLS
(with a GC reaction)
G
PFL-TLS
(FDCs, but no GC)
H
E-TLS
(no FDCs, no GC)
I
E-TLS
(mixed B and T cells)
CD21 CD23 CXCL13 DAPI
Autofluorescence
CD20 CD3
CXCL13 DAPI
J
DC+
HEV+
%
E-TLS
PFL-TLS
SFL-TLS
K
SFL-TLS
PFL-TLS
E-TLS
Unorganized infiltrate
CD21 CD23 PNAD CD20 DC-LAMP DAPI

Figure 1

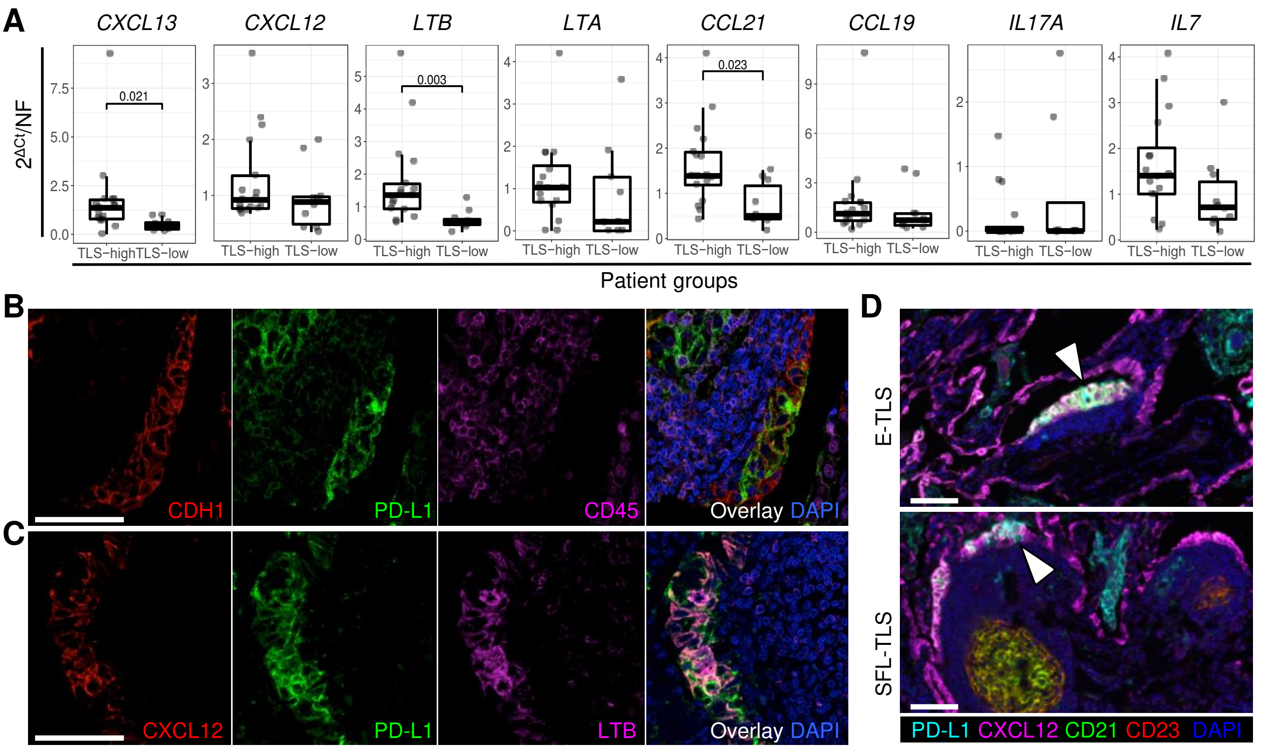

A
CXCL13
CXCL12
LTB
LTA
CCL21
CCL19
IL17A
IL7
2ΔCt/NF
0.021
0.003
0.023
TLS−high
TLS−low
Patient groups
B
CDH1
PD-L1
CD45
Overlay DAPI
C
CXCL12
PD-L1
LTB
Overlay DAPI
D
E-TLS
SFL-TLS
PD-L1 CXCL12 CD21 CD23 DAPI

Figure 2

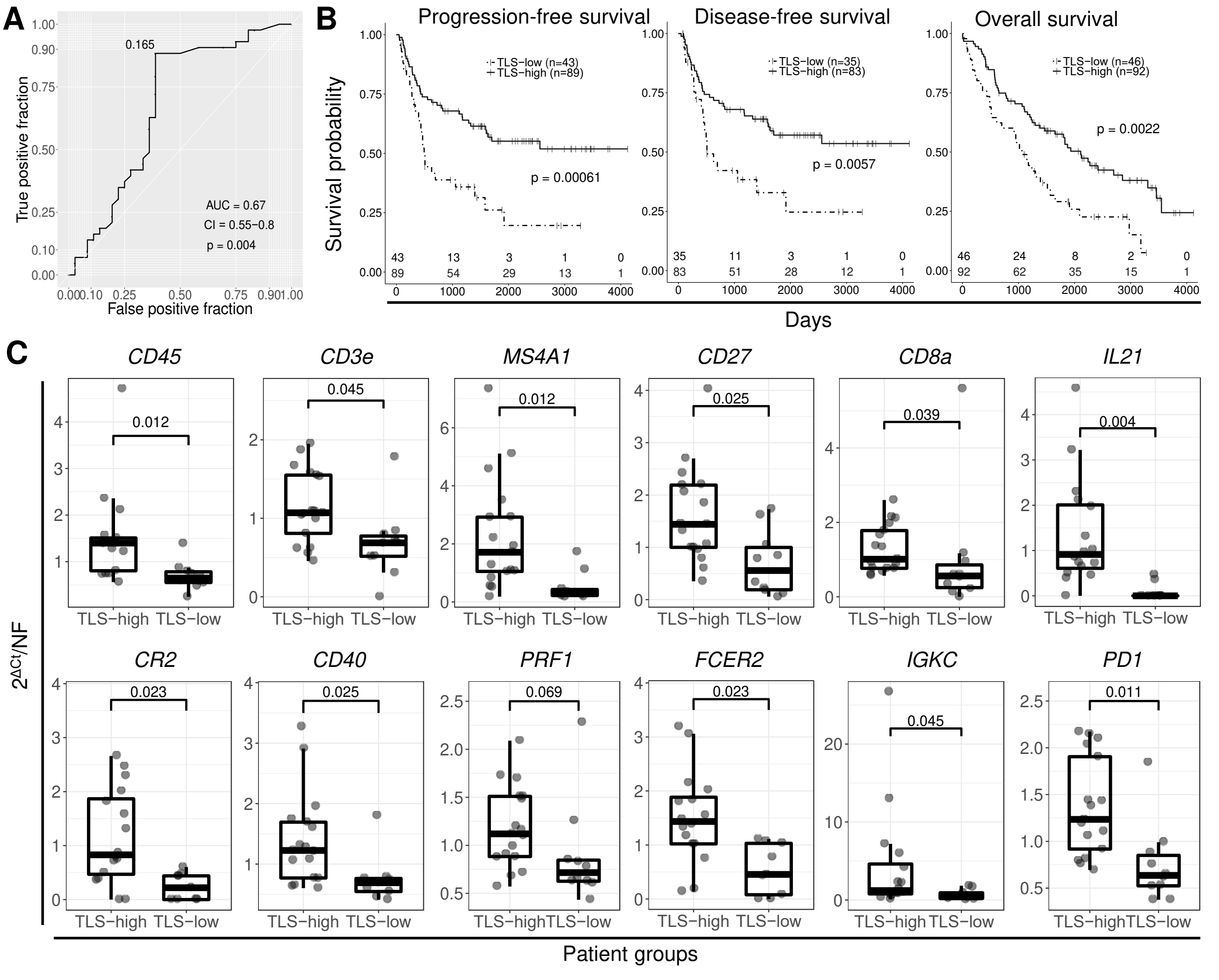
A
B
Progression-free survival
Disease-free survival
Overall survival
TLS−low (n=43)
TLS−high (n=89)
p = 0.00061
TLS−low (n=35)
TLS−high (n=83)
p = 0.0057
TLS−low (n=46)
TLS−high (n=92)
p = 0.0022
Survival probability
Days
0.165
AUC = 0.67
CI = 0.55−0.8
p = 0.004
True positive fraction
False positive fraction
C
CD45
CD3e
MS4A1
CD27
CD8a
IL21
CR2
CD40
PRF1
FCER2
IGKC
PD1
TLS−high
TLS−low
Patient groups

Figure 3

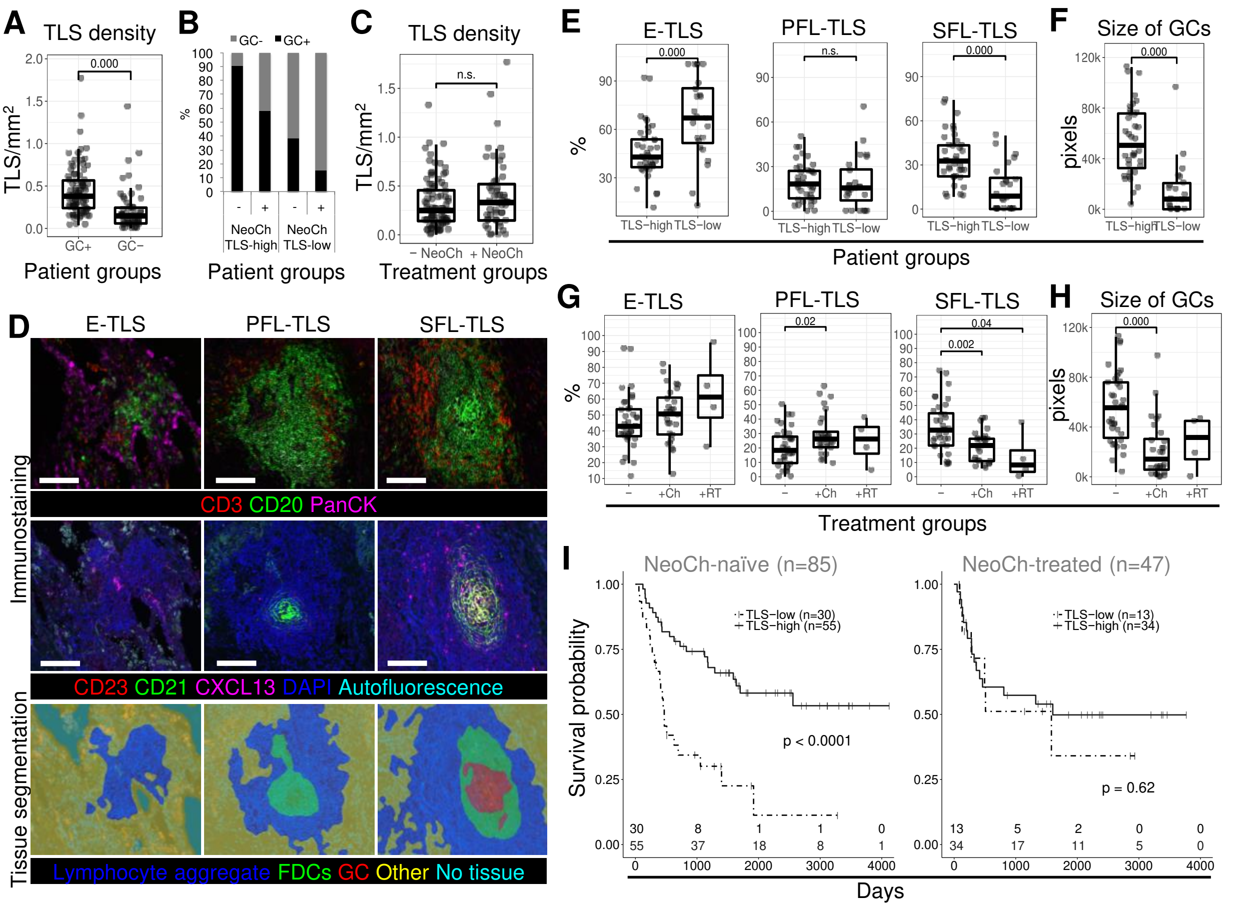

A TLS density
TLS/mm2
Patient groups
GC+ GC−
0.000
B
GC- GC+
NeoCh TLS-high
NeoCh TLS-low
Patient groups
C TLS density
TLS/mm2
n.s.
− NeoCh + NeoCh
Treatment groups
D E-TLS PFL-TLS SFL-TLS
Immunostaining
CD3 CD20 PanCK
CD23 CD21 CXCL13 DAPI Autofluorescence
Tissue segmentation
Lymphocyte aggregate FDCs GC Other No tissue
E E-TLS PFL-TLS SFL-TLS
F Size of GCs
TLS−high TLS−low
pixels
Patient groups
G E-TLS PFL-TLS SFL-TLS
H Size of GCs
− +Ch +RT
Treatment groups
I NeoCh-naïve (n=85)
NeoCh-treated (n=47)
TLS−low (n=30)
TLS−high (n=55)
TLS−low (n=13)
TLS−high (n=34)
Survival probability
p < 0.0001
p = 0.62
Days

Figure 4

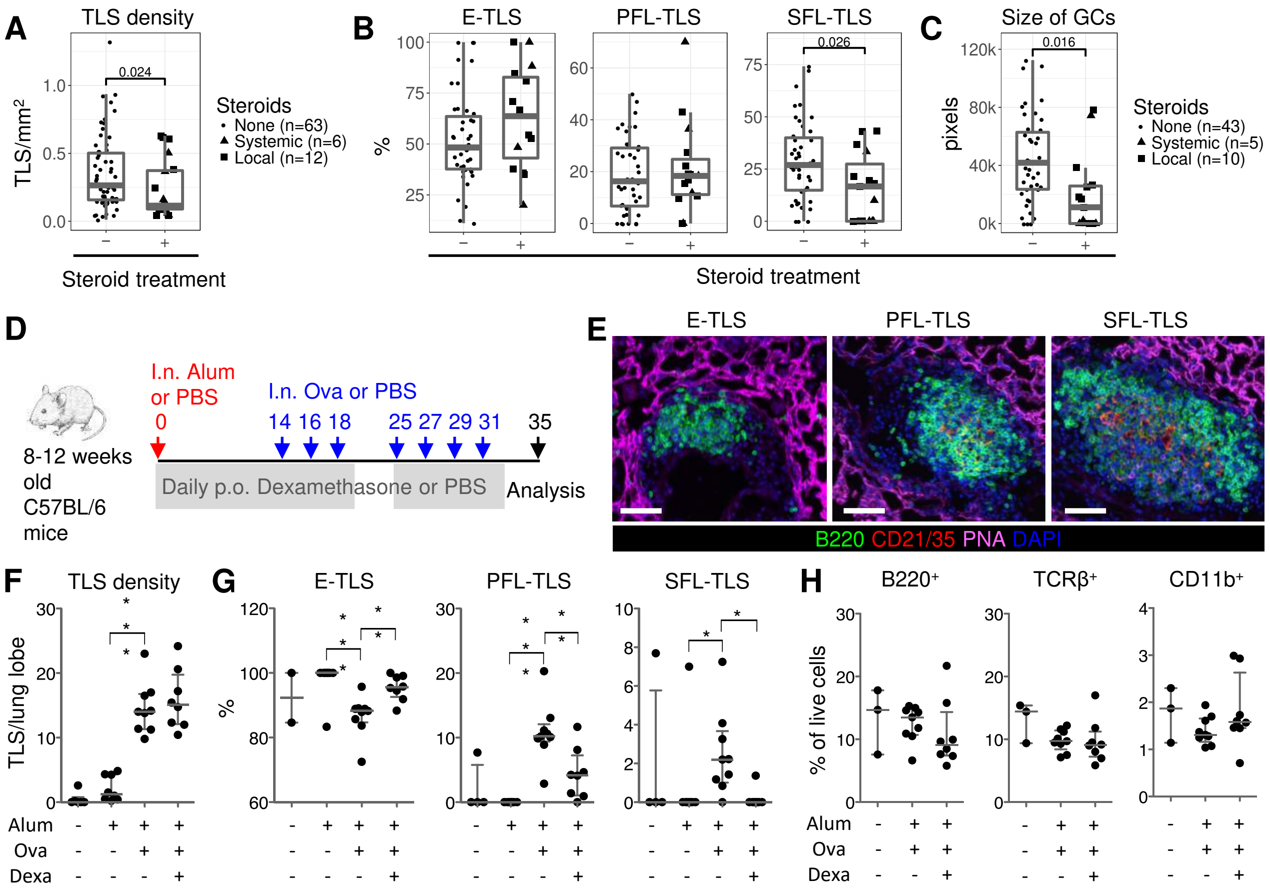

A
TLS density
TLS/mm2
0.024
Steroids
None (n=63)
Systemic (n=6)
Local (n=12)
Steroid treatment
B
E-TLS
PFL-TLS
SFL-TLS
%
0.026
Steroid treatment
C
Size of GCs
pixels
0.016
Steroids
None (n=43)
Systemic (n=5)
Local (n=10)
D
I.n. Alum or PBS
I.n. Ova or PBS
0
14 16 18
25 27 29 31
35
8-12 weeks old C57BL/6 mice
Daily p.o. Dexamethasone or PBS
Analysis
E
E-TLS
PFL-TLS
SFL-TLS
B220 CD21/35 PNA DAPI
F
TLS density
TLS/lung lobe
G
E-TLS
PFL-TLS
SFL-TLS
%
H
B220+
TCRβ+
CD11b+
% of live cells
Alum
Ova
Dexa

Figure 5

Author Manuscript Published OnlineFirst on December 26, 2017; DOI: 10.1158/0008-5472.CAN-17-1987
Author manuscripts have been peer reviewed and accepted for publication but have not yet been edited.

Cancer Research
The Journal of Cancer Research (1916–1930) | The American Journal of Cancer (1931–1940)

AACR American Association for Cancer Research

Germinal centers determine the prognostic relevance of tertiary lymphoid structures and are impaired by corticosteroids in lung squamous cell carcinoma

Karina Silina, Alex Soltermann, Farkhondeh Movahedian Attar, et al.

Cancer Res Published OnlineFirst December 26, 2017.

Updated version	Access the most recent version of this article at: doi:10.1158/0008-5472.CAN-17-1987
Supplementary Material	Access the most recent supplemental material at: http://cancerres.aacrjournals.org/content/suppl/2017/12/23/0008-5472.CAN-17-1987.DC1
Author Manuscript	Author manuscripts have been peer reviewed and accepted for publication but have not yet been edited.